Clim Dyn
DOI 10.1007/s00382-016-3298-x

Influence of seaway changes during the Pliocene on tropical Pacific climate in the Kiel climate model: mean state, annual cycle, ENSO, and their interactions

Zhaoyang Song[1] · **Mojib Latif**[1,2] · **Wonsun Park**[1] · **Uta Krebs-Kanzow**[3] · **Birgit Schneider**[2]

Received: 13 May 2016 / Accepted: 25 July 2016

Abstract The El Niño/Southern Oscillation (ENSO) is the leading mode of tropical Pacific interannual variability in the present-day climate. Available proxy evidence suggests that ENSO also existed during past climates, for example during the Pliocene extending from about 5.3 million to about 2.6 million years BP. Here we investigate the influences of the Panama Seaway closing and Indonesian Passages narrowing, and also of atmospheric carbon dioxide (CO_2) on the tropical Pacific mean climate and annual cycle, and their combined impact on ENSO during the Pliocene. To this end the Kiel Climate Model), a global climate model, is employed to study the influences of the changing geometry and CO_2-concentration. We find that ENSO is sensitive to the closing of the Panama Seaway, with ENSO amplitude being reduced by about 15–20 %. The narrowing of the Indonesian Passages enhances ENSO strength but only by about 6 %. ENSO period changes are modest and the spectral ENSO peak stays rather broad. Annual cycle changes are more prominent. An intensification of the annual cycle by about 50 % is simulated in response to the closing of the Panama Seaway, which is largely attributed to the strengthening of meridional wind stress. In comparison to the closing of the Panama Seaway, the narrowing of the Indonesian Passages only drives relatively weak changes in the annual cycle. A robust relationship is found such that ENSO amplitude strengthens when the annual cycle amplitude weakens.

Keywords Gateway · Panama Seaway · Indonesian Passages · Paleoclimate modeling · Annual cycle · ENSO

1 Introduction

Proxy data suggests the El Niño/Southern Oscillation (ENSO), the leading mode of present-day tropical interannual variability, was active across a wide variety of past climate states as far back as the late Cretaceous, Eocene, Miocene, Pliocene, Pleistocene and the Holocene (Davies et al. 2012; Huber and Caballero 2003; Galeotti et al. 2010; Watanabe et al. 2011; Scroxton et al. 2011; Cobb et al. 2003; McGregor et al. 2013). The Pliocene was the last period that featured an atmospheric CO_2-concentration which was similar to the present-day values, with concentrations amounting to about 405 ppm (Haywood et al. 2011). Paleogeochemical proxies indicate that sea surface temperature (SST) within the tropical warm pool regions may have changed little over the last 3 to 5 million years (Wara et al. 2005; Pagani et al. 2009). On the other hand, the cold tongue in the eastern equatorial Pacific was about 4–5 °C warmer than today (Wara et al. 2005; Fedorov et al. 2006) and SSTs in the subtropical upwelling zones were substantially warmer than the present (Brierley et al. 2009). The proxy records suggest that much reduced zonal and meridonal SST gradients existed in the early Pliocene (Wara et al. 2005; Fedorov et al. 2013). Although the SST gradient strengthened as

Electronic supplementary material The online version of this article (doi:10.1007/s00382-016-3298-x) contains supplementary material, which is available to authorized users.

✉ Zhaoyang Song
zsong@geomar.de

[1] GEOMAR Helmholtz Centre for Ocean Research Kiel, Kiel, Germany

[2] Excellence Cluster "The Future Ocean" at Kiel University, Kiel, Germany

[3] Alfred Wegener Institute Helmholtz Centre for Polar and Marine Research, Bremen, Germany

Published online: 03 August 2016

time progressed, it was still considerably reduced in the mid-Pliocene, which is thought to have had significant consequences for the tropical Pacific climate at that time, especially for ENSO.

Wara et al. (2005) referred the much warmer cold tongue in the eastern equatorial Pacific, which considerably reduces the zonal SST gradient, to as "permanent El Niño-like" conditions. Haywood et al. (2007) and Fedorov et al. (2010) report weak extant ENSO variations in coupled climate models. In contrast, proxy data and other modeling results suggest persistent significant ENSO variability. Proxy evidence suggesting persistent ENSO activity during the Pliocene has been provided by Watanabe et al. (2011) and Scroxton et al. (2011). Climate model simulations from the Pliocene Model Intercomparison Project (PlioMIP) yield ENSO variability simulated under reconstructed mid-Pliocene conditions (Haywood et al. 2011; Dowsett et al. 2012; Brierley 2015). Manucharyan and Fedorov (2014) simulate a robust ENSO under very different climatological zonal SST gradients. They manipulate the east–west equatorial Pacific SST gradient decreasing it from 6.0 to 1.4 °C, while the amplitude of ENSO decreases by only 30–40 %. How do these so called permanent El Niño-like tropical Pacific mean states maintain a "healthy" ENSO?

The opening and closing of oceanic gateways has a profound influence on the distribution of fresh water, nutrients, and energy in the global ocean, and is thus a major factor in driving past global environmental and climate changes. Here we investigate by means of a global climate model, the Kiel Climate Model (KCM, Park et al. 2009), the influences of the Panama Seaway closing and Indonesian Passages narrowing during the Pliocene on tropical Pacific mean climate, annual cycle and interannual variability. A particular focus is ENSO which, in simple nonlinear models, can be understood as the first (Hopf) bifurcation (Jin et al. 1996), moving the system from a stable to an oscillatory regime, when increasing the strength of ocean–atmosphere coupling which in turn is related to the zonal SST gradient. The tropical Pacific is special among the tropical oceans exhibiting a strong zonal asymmetry in its upper ocean thermal structure, which is clearly seen in the equatorial SST. In the western warm pool region SSTs amount to up to 29 °C, in the eastern cold tongue region SSTs are typically up to 10 °C colder. It is this zonal asymmetry that enables ENSO. In the central-eastern equatorial Pacific, variations in thermocline depth modulate SST through vertical advection of temperature anomalies by the mean upwelling—a process referred to as "thermocline feedback"—thereby communicating subsurface temperature signals to the surface. This introduces changes in the zonal SST gradient along the equator, which in turn interacts with the easterly trade winds (Bjerknes 1969), giving rise to a positive feedback. In conjunction with delayed negative feedbacks by the wind-driven ocean circulation and oceanic waves, these processes are at the heart of the ENSO mechanism.

How the character of ENSO changes when the tropical Pacific mean state changes is an important question. To assess the overall stability of ENSO in state-of-the-art climate models, Jin et al. (2006) proposed the Bjerknes stability (BJ) Index. This index has been used to investigate a large range of ENSO behaviors in and among coupled general circulation models (CGCMs) under a variety of background ocean–atmosphere mean states (e.g.; Kim and Jin 2010a, b), which aided the understanding of ENSO dynamics in climate models. The BJ index has also been applied to observations to understand differences between the equatorial Pacific and equatorial Atlantic interannual variability and shifts in ENSO behavior during the most recent decades (Lübbecke and McPhaden 2013, 2014).

Another important factor in determining the character of ENSO is the annual cycle, which is readily seen, for example, by the seasonal phase locking of ENSO with strongest SST anomalies in boreal winter and weakest in boreal spring. The annual cycle involves the development and decay of the eastern equatorial Pacific cold tongue, which is forced by the solar radiation in the first place. At the equator, however, the solar radiation exhibits a semiannual cycle. Yet the SST in the eastern and central Pacific depicts a pronounced annual cycle. The northerly position of the Intertropical Convergence Zone (ITCZ), owing to the hemispheric asymmetry of land–sea distribution, generates a weak annual cycle of surface wind forcing at the equator (Li and Philander 1996). One important mechanism in the equatorial annual cycle is the propagation of annual cycle signal from the South America coast through the Wind-Evaporation-SST (WES) feedback and the subsequent coupled ocean–atmosphere disturbance, as first pointed out by Liu and Xie (1994) and Liu (1996). Additionally, coupled air–sea feedbacks intensify the wind forcing by invoking a near-annual frequency mode that propagates westward (Li and Philander 1996; Xie 1996). Through the mechanism of frequency entrainment, the tropical annual cycle interacts with and tends to damp ENSO (Liu 2002; Chang et al. 1994).

In this study, we describe the sensitivity of the KCM's mean state, annual cycle and ENSO to external changes during the Pliocene, forced by changes in ocean geometry and atmospheric CO_2, Special attention is given to the influence of the Panama Seaway closing and Indonesian Passages narrowing, and to the interaction between the annual cycle and ENSO. The structure of this paper is as follows. In Sect. 2, we describe the coupled model and the experimental design. Mean state changes are presented in Sect. 3. The response of the SST annual cycle is addressed in Sect. 4. In Sect. 5, ENSO stability is discussed on the

basis of the BJ Index. We conclude this paper with a brief summary and a discussion of the main results in Sect. 6.

2 Coupled model, experimental setup, and methods

2.1 Coupled model and experiment setup

We use the Kiel Climate Model (KCM, Park et al. 2009). The atmosphere model is ECHAM5 (Roeckner et al. 2003) which is integrated with T31 (3.75° × 3.75°) horizontal resolution and 19 vertical levels up to 10 hPa. The ocean-sea ice component is NEMO (Madec 2008) on a 2° Mercator mesh, with 31 vertical levels. The meridional resolution increases towards lower latitudes, with 0.5° in the equatorial region. The two components are coupled with the OASIS3 coupler (Valcke 2006). No form of flux correction or anomaly coupling is employed. The KCM has been applied in studies addressing past, present-day and future climate. A list of references of published studies employing the KCM can be obtained from http://www.geomar.de/en/research/fb1/fb1-me/research-topics/climate-modelling/kcms/.

In terms of gross indices, ENSO is simulated reasonably well by the KCM, as described in Park et al. (2009) and more recently, in Latif et al. (2015). The ENSO response of the KCM to strongly increasing atmospheric CO_2 has also been described in Park et al. (2009) and Latif et al. (2015). The tropical Pacific response to increasing greenhouse gas concentrations in other climate models, which participate in the Coupled Model Intercomparsion Project phase 3 (CMIP3) and phase 5 (CMIP5), and in the Pliocene Model Intercomparison Project (PlioMIP), has been explored, for example, in Latif and Keenlyside (2009), DiNezio et al. (2012), Collins et al. (2010), Bellenger et al. (2014) and Brierley (2015). In comparison to those models, the KCM is somewhat special, as it projects strongly increasing ENSO amplitude under global warming conditions (Fig. S1, S2, S3), which is mainly due to strengthened thermocline feedback and enhanced atmospheric sensitivity to SSTA (Park et al. 2009). Further, skewness and kurtosis also increase at higher CO_2 (Fig. S4).

A set of eight experiments is conducted (Table 1) in order to separate the climate effects of lowering atmospheric CO_2, narrowing of the Indonesian Passages and closing of the Panama Seaway, which happened during the Pliocene. Experiment names consist of three sequential letters representing different boundary conditions. The first letter indicates CO_2-concentration [Low (286 ppm) and High (405 ppm)], the second letter the Indonesian Passages [Modern or Pliocene geometry (wider and deeper than modern)], and the third letter the Panama Seaway [Modern (closed) or Pliocene geometry (open, with a depth 1200 m)]. For example, LMM represents the experiment with Low-CO_2 and Modern Indonesian Passages and Modern Panama Seaway, and this integration serves as a pre-industrial control simulation. LMM is integrated for 2000 years starting from the Levitus climatology of temperature and salinity. Experiment HMM differs from experiment LMM only in the CO_2-concentration which is higher. HMM serves as control run for the high-CO_2 experiments. The other six experiments are initialized with the output from either LMM or HMM and integrated for 800 years. The last 300-years from each of the integrations are used in the subsequent analysis.

The deeper and wider geometry of the Indonesian Passages during the Early Pliocene follows the assumption of Cane and Molnar (2001): the passages between Sulawesi and New Guinea are 1000 m deeper relative to the modern bathymetry, the northern coast of New Guinea is located 2° south due to the missing of the northern part, and the passage between Timor and Australia is also wider and deeper by removing part of Timor. Effects of such tectonic changes

Table 1 Overview of the model simulations analyzed in this paper

Experiment name	Atmospheric CO_2		Indonesian Passages		Panama Seaway		Integration
LMM	286 ppm	L	Modern	M	Closed	M	2000
LPM	286 ppm	L	Deep/wide	P	Closed	M	800
LMP	286 ppm	L	Modern	M	1200 m	P	800
LPP	286 ppm	L	Deep/wide	P	1200 m	P	800
HMM	405 ppm	H	Modern	M	Closed	M	1000
HPM	405 ppm	H	Deep/wide	P	Closed	M	800
HMP	405 ppm	H	Modern	M	1200 m	P	800
HPP	405 ppm	H	Deep/wide	P	1200 m	P	800

Acronyms of the experiments stand for Low (High) atmospheric CO_2-concentration, Modern (Pliocene) Indonesian Passages, Modern (Pliocene) Panama Seaway for the first, second, and third characters, respectively. HMM and LMM are the "present-day" control simulations with high and low CO_2-concentration, respectively

have been shown to cause the acidification off Australia and a series of complex Indo-Pacific climate changes (Krebs et al. 2011). An open Panama Seaway is accomplished in the model by replacing four land grid cells by ocean grid cells between North and South America located at approximately 8°N. We employ a depth of 1200 m representing a deep Panama Seaway to simulate the early stage of the shoaling process.

2.2 Amplitude equation for the annual cycle

With some modifications and systemic assumptions that filter out interannual variability signals, the governing mixed layer SST anomaly equation for the annual cycle over the equatorial eastern Pacific deduced by Xie (1994) is:

$$\frac{\partial T'}{\partial t} = -(\bar{u}_o - c)\frac{\partial T'}{\partial x} + \frac{2Q_s}{\rho C_p h} - \left(1 + \frac{\eta}{H}\right)\frac{2\bar{Q}_E}{\rho C_p h}\frac{\bar{v}}{|\bar{u}|^2}v' - \varepsilon T', \quad (1)$$

where T' is the SST anomaly (relative to the annual-mean SST) in the mixed layer, $\bar{u}_0$ denotes the mean zonal current velocity, c is the phase speed due to a 90° phase difference between the zonal wind stress and SST, and h the depth of the mixed layer. The relative importance between the mean latent heat flux and vertical mixing is measured by the ratio η/H; Q_S and $\bar{Q}_E$ are the perturbation solar radiation and the mean latent heat flux, respectively; $\bar{u}$ and $\bar{v}$ are the mean zonal and meridional wind stress, respectively. The constants ρ and c_p denote ocean density and heat capacity of sea water at constant pressure, respectively. ε is the thermal damping timescale. The first three terms on the right hand side indicate westward propagation via air–sea coupling, the surface solar radiation and the latent heat flux depending on changes in the meridional wind stress, respectively. The fourth term is surface radiative cooling. More details about Eq. (1) can be found in Xie (1994). For the derivation, see Anderson and McCreary (1985) and Xie et al. (1989). From Eq. (1), the westward propagation of the annual cycle signal is dominant at the equator where the meridional SST gradient vanishes. Meridional advection becomes more important off the equator due to the increasing meridional SST gradient.

An and Choi (2013) multiplied Eq. (1) by T' to derive the amplitude tendency equation:

$$\frac{\partial}{\partial t}\left\langle T'^2\right\rangle = -(\bar{u}_o - c)\frac{\partial}{\partial x}\left\langle T'^2\right\rangle + \frac{4}{\rho C_p h}\langle Q_S T'\rangle - \left(1 + \frac{\eta}{H}\right)\frac{4\bar{Q}_E}{\rho C_p h}\frac{\bar{v}}{|\bar{u}|^2}\langle v'T'\rangle - 2\varepsilon\left\langle T'^2\right\rangle, \quad (2)$$

As seen in Eq. (2), the annual cycle of SST in the eastern Pacific is largely controlled by the second and third term on the right hand side. Within a seasonal cycle, the solar forcing is positively correlated to SST (i.e. $\langle Q_S T'\rangle$ is positive), while the cross-equatorial southerly is negatively correlated to the SST [i.e. $\langle v'T'\rangle$ is negative, also see Fig. 6 in An and Choi (2013)]. Thus the amplitude of annual cycle is positively correlated to solar forcing $\left(\frac{\partial}{\partial t}\langle T'^2\rangle \propto \langle Q_S T'\rangle\right)$ in the second term, latent heat flux $\left(\frac{\partial}{\partial t}\langle T'^2\rangle \propto \bar{Q}_E \cdot -(\langle v'T'\rangle)\right)$, $v\left(\frac{\partial}{\partial t}\langle T'^2\rangle \propto \bar{v} \cdot -(\langle v'T'\rangle)\right)$ in the third term and negatively correlated to the mixed layer depth $\left(\frac{\partial}{\partial t}\langle T'^2\rangle \propto \frac{1}{h}\right)$ and zonal wind $\left(\frac{\partial}{\partial t}\langle T'^2\rangle \propto \frac{1}{|\bar{u}|^2} \cdot -(\langle v'T'\rangle)\right)$. The mixed layer depth (h) involves both terms; therefore it has somewhat stronger effect on the annual cycle of the SST. Detailed analysis using the output from the numerical experiments will be presented in Sect. 4.

2.3 Bjerknes stability index

We assess the characteristics of the ENSO mode in our experiments through quantifying the relative strength of positive and negative feedbacks by using the Bjerknes stability index derived by Jin et al. (2006) from the linear equation for SST anomalies in the mixed layer [Eq. (1) in Jin et al. (2006)]. The volume average of the linearized SST equation is taken over the upper eastern equatorial Pacific where the SST exhibits its maximum interannual variability.

The resulting equation obtained by applying several approximations is written as:

$$\frac{\partial \langle T\rangle_E}{\partial t} = 2\mathrm{I}_{BJ}\langle T\rangle_E + F[h], \quad (3)$$

where

$$2I_{BJ} = -\left(\frac{\langle \bar{u}\rangle_E}{L_x} + \frac{\langle -2y\bar{v}\rangle_E}{L_y^2} + \frac{\langle \bar{w}\rangle_E}{H_m}\right) - \alpha + \mu_a\beta_u\left\langle -\frac{\partial \bar{T}}{\partial x}\right\rangle_E + \mu_a\beta_w\left\langle -\frac{\partial \bar{T}}{\partial z}\right\rangle_E + \mu_a\beta_h\left\langle \frac{H(\bar{w})\bar{w}}{H_m}a_h\right\rangle_E, \quad (4)$$

and

$$F = \beta_{uh}\left\langle -\frac{\partial \bar{T}}{\partial x}\right\rangle + \left\langle \frac{H(\bar{w})\bar{w}}{H_m}\right\rangle_E a_h, \quad (5)$$

with $\langle\cdot\rangle_E$ denoting the volume average over the eastern equatorial Pacific box. Variables with an overbar indicate climatological means. T, u, v and w represent the SST anomalies, the zonal, meridional and vertical velocity anomalies, respectively; and Q $\left(\alpha = \frac{\langle Q\rangle}{\langle T\rangle}\right)$ denotes the anomalous net heat flux from the atmosphere into the ocean and diffusive processes. The zonal and meridional extents of the eastern equatorial box are L_x and L_y, y is the distance from the

equator. The factor $-2y/L_y$ comes from the assumption that the meridional structure of ENSO-related SST anomalies is Gaussian-like with an e-folding decay scale of L_y. The depth H_m is the effective depth for vertical advection, α the linear estimation of thermal damping and μ_a the zonal wind stress response to SST forcing. β_u, β_w and β_h describe the ocean surface current, the upwelling and thermocline slope to equatorial zonal wind forcing, respectively. β_{uh} is the geostrophic adjustment of zonal currents to the thermocline depth anomalies, a_h the subsurface temperature change response to thermocline depth variations. The step function $H(x)$ ensures that only upward vertical motion affects surface temperature. The Bjerknes stability index is denoted by I_{BJ}, while F is a phase transition term associated with the recharge/discharge of the heat content. The terms of the BJ Index in Eq. (4) describe either negative or positive feedbacks involved to damp or enhance an SST anomaly in the eastern equatorial Pacific. From left to right the first two terms that make negative contributions correspond to dynamical (mean zonal advection and upwelling) and thermal damping, while the last three terms describing positive feedbacks are the zonal advection, Ekman pumping and thermocline feedback. A negative BJ Index is associated with a stable, damped system, and vice versa.

The computation of the BJ Index is sensitive to the region over which the variables are averaged. The longitudinal range of the volume average boxes that are indicated by $\langle\cdot\rangle_E$ and $\langle\cdot\rangle_W$ are defined as 120°E–180°, 5°S–5°N and 180°–80°W, 5°S–5°N within the mixed layer, respectively. Thus, the Niño-3 region, the area of strongest interannual SST variability (see Fig. 6), is accounted for in the eastern volume average box. The vertical range is from the surface to the bottom of the mixed layer. The mixed layer depth in the model is estimated by a Richardson number–dependent mixing parameterization, with a density threshold of 0.01 kg m^{-3}. In this study, we employ the depth of the 20 °C isotherm (Z20) to represent the thermocline depth. Interannual anomalies are computed by subtracting a mean seasonal cycle from all time-series after detrending them.

3 Simulated mean tropical climate

Under preindustrial conditions (LMM: low CO_2, modern oceanic passages), a warm pool with SSTs exceeding 29 °C is simulated in the west and a cold tongue in the east, which together allow for strongly zonally asymmetric tropical Pacific SSTs (Fig. 1a). The simulated preindustrial SSTs are considerably colder compared to those simulated for the early Pliocene (HPP: high CO_2, wide Indonesian Passages, open Panama Seaway), as shown in Fig. 1b. Exceptions are limited regions in the North Pacific and North Atlantic, which depict warmer SSTs under preindustrial conditions. The generally warmer SSTs simulated for the early Pliocene must be due to the combined effects of enhanced atmospheric CO_2 and altered oceanic passages. The open Panama Seaway yields weaker Atlantic Meridional Overturning Circulation (AMOC) and Kuroshio Current (Maier-Reimer et al. 1990), which accounts for the cooler SSTs in parts of the North Atlantic and North Pacific.

This study mainly focuses on the SST changes due to seaway change. Figure 2 shows global SST differences between the different experiments which differ in the geometry of the Indonesian and/or Panama Seaways, or CO_2 concentration. Relative to the deep and wide Indonesian Passages (LPM) run, the pre-industrial control run (LMM) with narrower and shallower Indonesian Passages depicts small surface warming in the Pacific warm pool area and cooling in the eastern Indian Ocean warm pool area, with SST changes amounting to well below 1 °C for low atmospheric CO_2 (Fig. 2a). The stronger SST response (Fig. 2b) to narrowing the Indonesian Passages is probably due to the considerably stronger ocean circulation changes at higher CO_2 (Fig. S5). The closed Panama Seaway experiments, independent of the CO_2-concentration (LPM, Fig. 2c; HPM, Fig. 2d), generally yield stronger SST changes. In the equatorial Pacific, a meridional dipole is observed, which is strongest in the east, with cooling south and warming north of the equator (Fig. 2c, d). The Pacific warm pool area becomes warmer, but by less than 1 °C. Relatively strong changes are seen in the extratropical oceans. SSTs in the North Pacific and North Atlantic increase by 2 °C or by even more in localized regions. The warming in the North Atlantic is due to enhanced northward heat transport associated with a stronger Atlantic Meridional Overturning Circulation (AMOC) (not shown). This is supported by the cooling of the South Atlantic, which together with the North Atlantic warming is a typical signature of AMOC strengthening in climate models (Latif et al. 2004) and referred to as the Interhemispheric Dipole (e.g., Folland et al. 1986). The closed Panama Seaway prevents fresher water being transported from the Pacific into the Atlantic, which eventually enhances the formation of North Atlantic Deep Water (NADW). The influences of the closed Panama Seaway on North Atlantic sector climate and the corresponding mechanisms have been discussed from a multi-model perspective in Zhang et al. (2012). The influence of the Panama Seaway closing on the AMOC in the KCM and its potential role in Northern Hemisphere glaciation will be the subject of a forthcoming paper.

When the Indonesian Passages and Panama Seaway are changed together towards modern conditions (Fig. 2e, f), the SST responses are very similar to those of the Panama Seaway-closing experiment, indicating much stronger

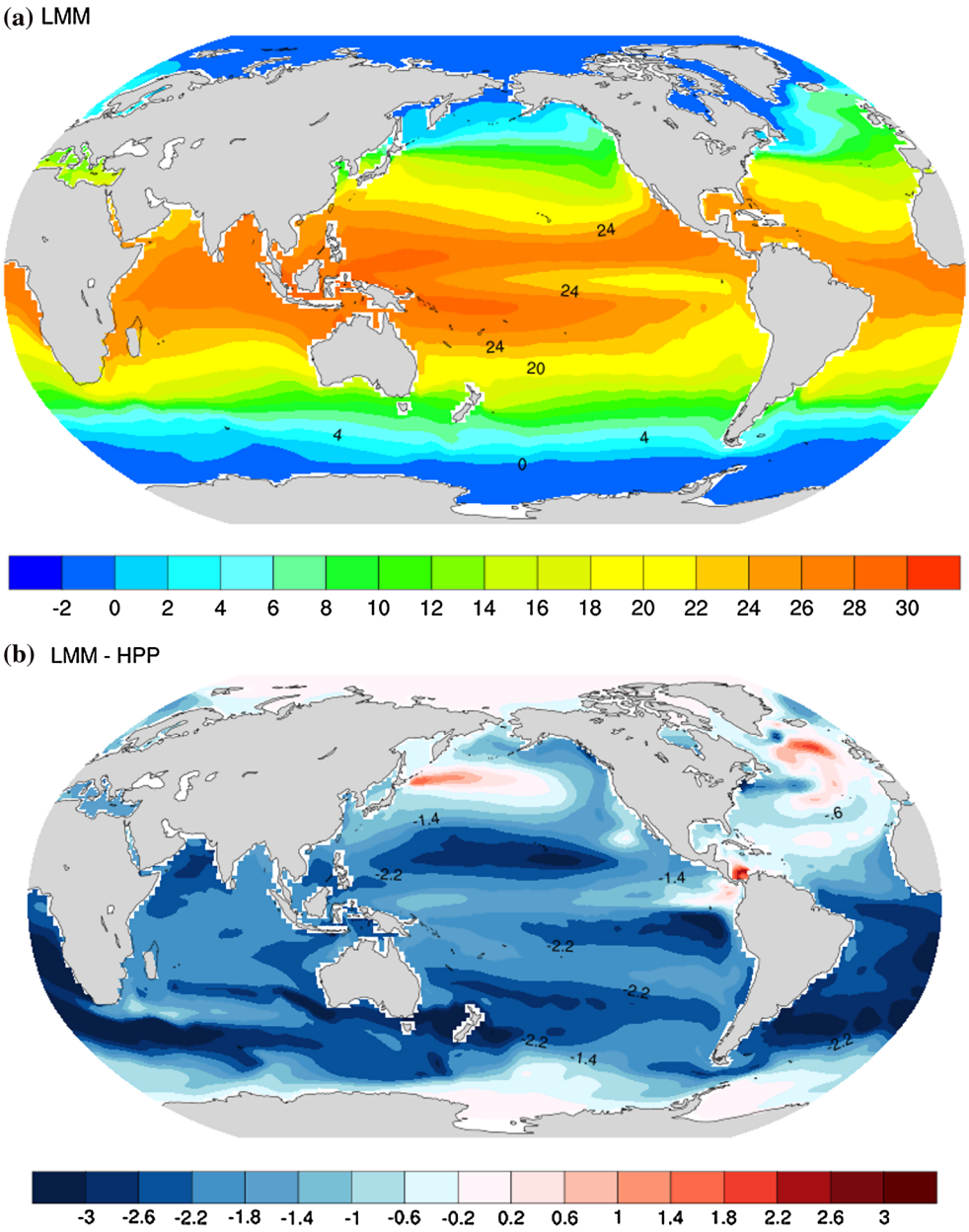

Fig. 1 **a** Climatology of SST (°C) in the pre-industrial control simulation LMM (low-CO_2, modern ocean geometry). **b** Difference between LMM and HPP (high-CO_2, wide and deep Indonesian Passages and open Panama Seaway). 300 years from each experiment were used in the calculations. Experiment HPP represents early Pliocene conditions

influences of the Panama Seaway change. In the equatorial Pacific, the warming is slightly larger when both passages are changed simultaneously in the KCM. Not much dependence on the CO_2-concentration is found; the SST patterns are quite similar in the low—(Fig. 2, left panels) and high-CO_2 (Fig. 2, right panels) simulations.

We next analyze thermocline depth in the tropics (30°N–30°S), as represented by the depth of the 20 °C isotherm (Z20, Fig. 3). The field of mean Z20 (Fig. 3b) simulated by the KCM under present-day conditions is compared to observations in Park et al. (2009) (see Fig. 5 therein). The narrower Indonesian Passages mainly shoals the Z20 in the Indonesian Throughflow region (Fig. 3c, d) and deepens the thermocline elsewhere, with largest deepening in the subtropics of all three tropical oceans. A generally stronger Z20-response is observed when the Panama Seaway is closed. Shallower Z20 is simulated in the tropical Indian Ocean, especially in its southern part, mainly due to constrained heat transport associated with the Indonesian Throughflow narrowing (Fig. 3c, d). In the tropical Pacific, Z20 shoals north of the equator and deepens south of the equator owing to decreased mixing of Pacific and Atlantic waters. In the tropical Atlantic, on the other hand, the Z20 deepens north of the equator but shoals to the south owing to enhanced northward heat transport associated with stronger AMOC. The strongest change in Z20 is observed in the North Atlantic depicting much deeper mixed layer depths.

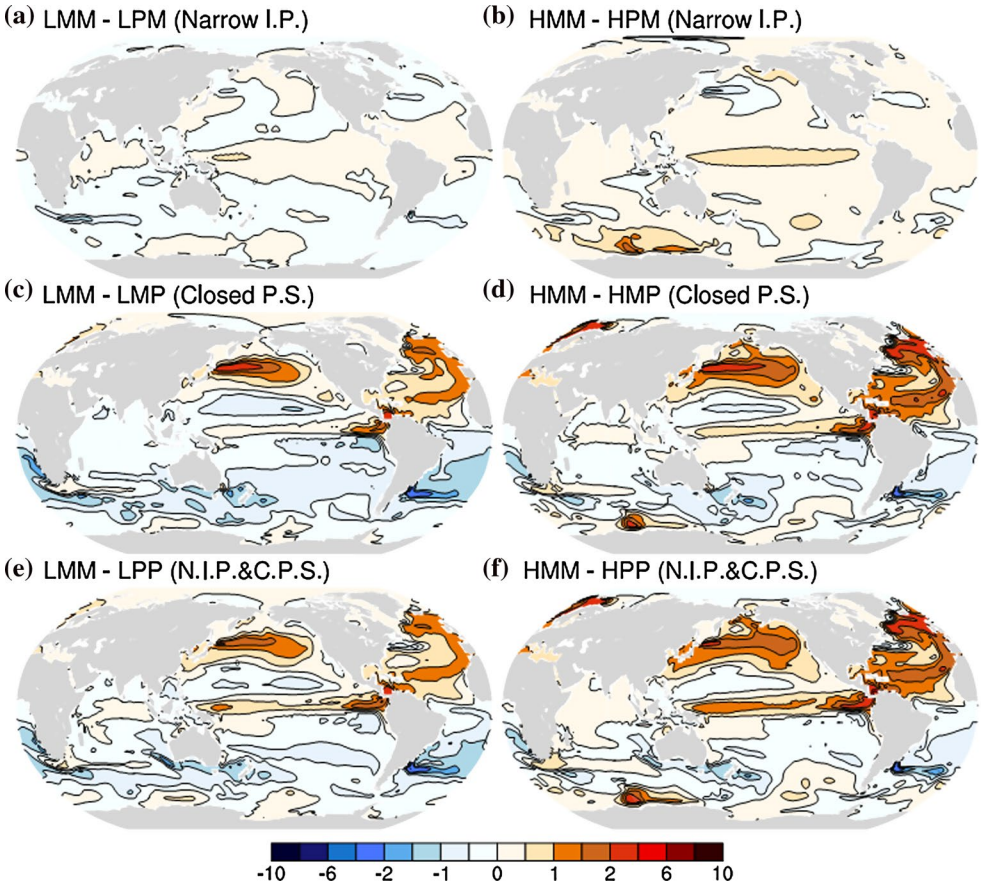

Fig. 2 SST (°C) responses to changes in topography with respect to the control simulation LMM employing low CO_2-concentration (*left panels*; **a**, **c**, **e**) and HMM employing high CO_2-concentration (*right panels*; **b**, **d**, **h**), due to **a**, **b** the narrowing of the Indonesian Passages, **c**, **d** closing of the Panama Seaway, and **e**, **f** due to both changes in ocean geometry. The *contour intervals* are 0.5 °C in the range of −2 to 2 °C and 2 °C in the range of 2 to 10 °C, respectively

Mean-state changes are also prominent in other oceanic and atmospheric variables (Fig. 4). Figure 4a displays the meridionally averaged (5°S–5°N) annual-mean equatorial Pacific SSTs. All three runs with geographical changes towards modern conditions yield warmer equatorial Pacific SSTs, with the experiment HMM (high CO_2, modern oceanic passages) providing the warmest equatorial Pacific SSTs. Warmer temperatures generally go along with weaker easterly zonal wind stress over the eastern and central equatorial Pacific (Fig. 4b) and stronger northward meridional wind stress (Fig. 4c). The latter explains the north–south asymmetry in the equatorial SST response. Consistent with the weaker easterly zonal wind stress equatorial thermocline (Z20) tilt is reduced. The Z20 shoals in the west and to a lesser degree also in the east (Fig. 4d); the overall shoaling of Z20 indicates a substantial subsurface cooling due to the closing of the Panama Seaway (Karas et al. 2009).

Figure 5 depicts the simulated annual cycle of SST along the equatorial Pacific (averaged over 5°S–5°N) for each experiment (upper panels: low-CO_2 experiments, lower panels: high-CO_2 experiments). In all experiments and consistent with present-day conditions, there is an annual cycle in the east and a semi-annual cycle in the west. However, the amplitude of the semi-annual and annual cycle considerably varies among the experiments. The annual cycle amplitude is defined here as the difference between the maximum and the minimum SST anomaly relative to the annual mean (Bellenger et al. 2014; Table 2). Both the closing of the Panama Seaway and the narrowing of the Indonesian Passages can increase the annual cycle amplitude. In the four open-Panama Seaway runs (Fig. 5c, d, g, h), the annual cycle amplitude is relatively weak amounting to 1.09, 0.77, 1.28 and 0.84 °C in experiments LMP, LPP, HMP and HPP (Table 2), respectively. In response to the closing of the Panama Seaway (Fig. 5a, b, e, f), the amplitude of the SST annual cycle in the eastern equatorial Pacific increases, with values up to 2.00 and 1.93 °C in the experiments HMM and LMM, respectively. We note, however, that all simulations are biased with respect to the present-day SST annual cycle, with the cold tongue in the east not being maintained until the end of the calendar year. The simulation of the SST annual cycle in the eastern equatorial Pacific is a long-standing problem in climate models (e.g., Mechoso et al. 1995).

The changes in the annual cycle have the potential to modify ENSO. In fact, the level of ENSO variability, as shown by the standard deviation of the monthly SST anomalies, varies considerably among the simulations (Fig. 6). The ENSO amplitude, defined here as the standard

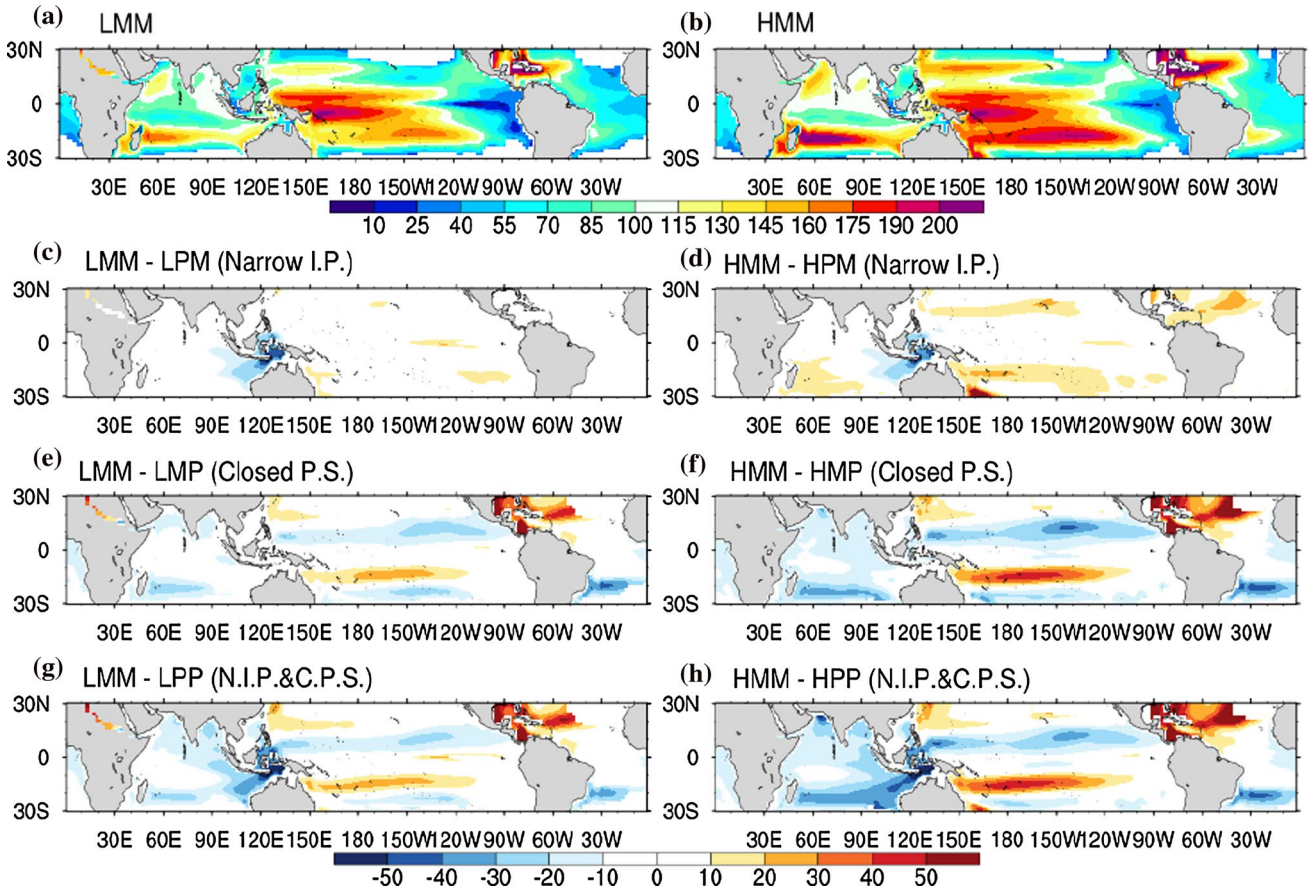

Fig. 3 Annual-mean depth (m) of the 20 °C isotherm (Z20) in the control experiment **a** LMM and **b** HMM (*contour interval* 15 m). **c–h** Z20-changes in the simulations with low/high-CO_2 and different ocean geometry with respect to LMM/HMM (*contour interval* 10 m)

deviation of the monthly SST anomalies averaged over the Niño3 region (90°W–150°W, 5°S–5°N), in the open Panama Seaway experiments LMP, HMP, LPP and HPP amount to 0.99, 1.07, 1.00, and 1.04 °C, respectively. Closing the Panama Seaway induces weaker ENSO variability. The ENSO amplitude in experiments LMM (Fig. 6a) and HMM (Fig. 6b) reduces to 0.85 and 0.91 °C, respectively. Yet it is stronger than the wider-Indonesian Passages experiments LPM and HPM in which the ENSO amplitude is 0.80 and 0.90 °C, respectively. The strength of strong events remains relatively stable in the experiments (not shown). The spectra of the monthly SST anomalies averaged over the Niño3 region depict significant peaks at interannual timescales (Fig. 7), for low (Fig. 7a) and high (Fig. 7b) atmospheric CO_2. No significant changes in ENSO period are seen across the ensemble of experiments, indicating sensitivity of ENSO with respect to amplitude but not period.

In the following we investigate the changes in ENSO dynamics in more detail. This part benefits from extensive previous work on tropical climate changes with regard to the mean state, oceanic and atmospheric feedbacks, ocean adjustment processes and annual cycle, and response to global warming (e.g., Latif and Keenlyside 2009; Collins et al. 2010; Vecchi and Soden 2007; Timmermann et al. 2007; Huang 2015).

4 Annual cycle response

We start with the response of the annual cycle (Fig. 5), because the annual cycle strongly influences ENSO, as expressed, for example, by the seasonal phase locking of ENSO. The KCM simulates a considerably strengthened annual cycle in the eastern equatorial Pacific in response to the closing of the Panama Seaway, independent of the CO_2 concentration (Fig. 5b, d; experiments LPM and HPM). Utilizing the amplitude tendency equation [Eq. (2)] deduced by An and Choi (2013), we address the physical mechanisms responsible for the enhancement in the amplitude of the SST annual cycle in eastern equatorial Pacific relative to the early Pliocene. Specifically, the effects of altered zonal and meridional surface winds, equatorial SST gradient and mixed layer depth are examined.

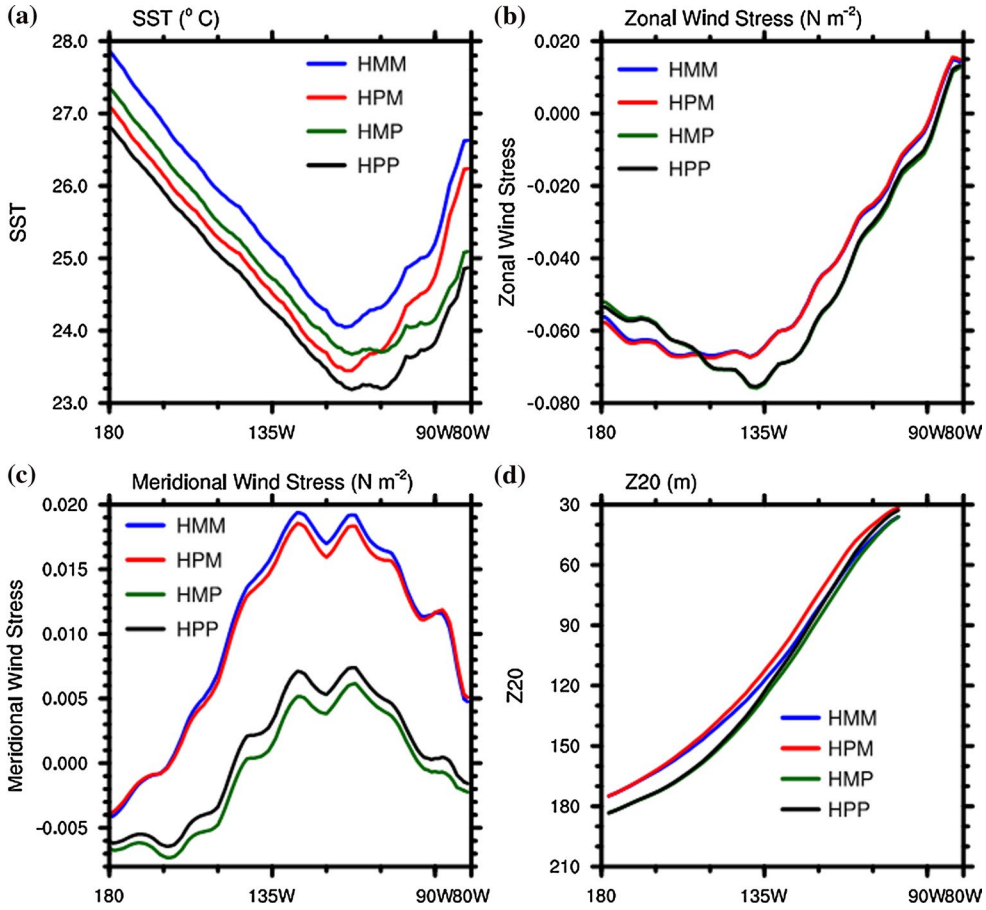

Fig. 4 Annual-mean values of selected variables along the equator (5°S–5°N) in the simulations with high CO_2. **a** SST (°C), **b** zonal wind stress (Nm^{-2}), **c** meridional wind stress (Nm^{-2}), **d** depth (m) of 20 °C isotherm (Z20)

Forced by annual variations in solar radiation off the equator, the annual variability is initiated along the South American coast, exhibiting its largest amplitude near 15°S. The signal propagates to the equator and to the west due to surface ocean–atmosphere interactions. At the equator, the annual cycle is related to the SST gradient, determined by the Walker circulation, and zonal currents in the mixed layer (Xie 1996). The first term on the right hand side of Eq. (2) denotes the westward propagation of the annual cycle. It can be inferred from Fig. 4b that the zonal wind stress in the east decreases in response to the Panama Seaway closing (i.e., difference between experiments HMM and HMP). The surface zonal winds change due to air–sea interaction. More specifically, the closing of the Panama Seaway reduces the zonal winds east of 150°W and intensifies them to the west (Fig. 4b). The most prominent changes are seen in the surface meridional winds (Fig. 5c). In the experiments with a closed Panama Seaway (HMM and HPM), the KCM simulates much stronger meridional winds, which is key to the existence of an SST annual cycle (AC) at the equator.

Stronger surface meridional winds (given the negative correlation between surface meridional wind and SST within a seasonal cycle) drive a stronger AC (and vice versa) according to Eq. (2) $\left(\frac{\partial}{\partial t}\langle T'^2\rangle \propto \bar{v}\cdot -\left(\langle v'T'\rangle\right)\right)$. Changes in the mean surface meridional wind ($\bar{v}$) modify the surface latent heat flux thereby also affecting the amplitude of the AC. The closing of the Panama Seaway, on the other hand, substantially develops the meridional SST gradient (Fig. 2c–f) and surface meridional winds in the east. The latter is seen in the annual-mean meridional wind (southerly) stress which increases by more than 30 % in response to the closing of Panama (Fig. 4c). Thus, the AC is substantially intensified under the enhanced southerly wind induced by the closing of the Panama Seaway. Narrowing the Indonesian Passages (i.e., difference between experiments HMM and HPM) hardly modifies the zonal SST gradient in the east. This geometry change mainly modifies the strength of the throughflow in the western Pacific, which hardly influences the eastern equatorial Pacific SST (Fig. 2a, b).

As indicated in Eq. (2), deeper mixed layer depth suppresses the amplitude of the AC, because its growth rate is inversely proportional to the mixed layer depth $\left(\frac{\partial}{\partial t}\left\langle T'^2\right\rangle \propto \frac{\langle Q_S T'\rangle}{h} \text{ and } \frac{\partial}{\partial t}\left\langle T'^2\right\rangle \propto \frac{\bar{Q}_E}{h}\cdot -\left(\langle v'T'\rangle\right)\right)\cdot$ The effect of solely narrowing the Indonesian Passages

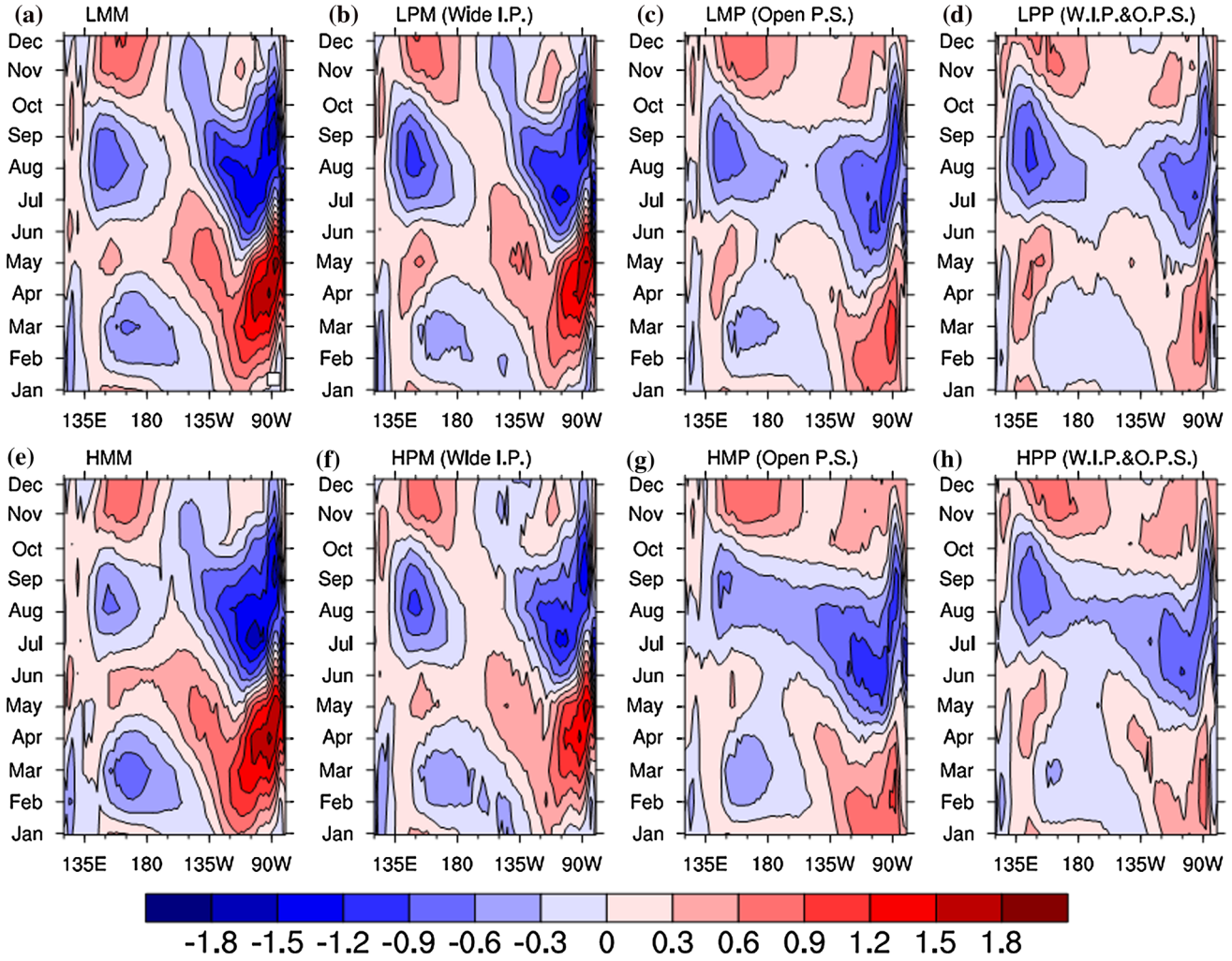

Fig. 5 Seasonal cycle (departure from the annual mean) of SST (°C) along the equatorial Pacific (averaged over 5°S–5°N latitudinal band) in the simulations with **a**–**d** low and **e**–**h** high CO_2 and different ocean geometries (*contour interval* 0.2 °C)

Table 2 The amplitude of annual cycle in the east equatorial Pacific (EEP) is summarized

Experiment name	Annual cycle amplitude (°C)
LMM	1.93
LPM	1.58
LMP	1.09
LPP	0.77
HMM	2.00
HPM	1.42
HMP	1.28
HPP	0.84

The amplitude of annual cycle in EEP is defined as the difference between the maximum and minimum Niño3 (150°W–90°W, 5°S–5°N) domain-averaged monthly mean SST anomalies in relative to the climatological annual mean

(e.g., HMM minus HMP) hardly modifies the mixed layer depth (expressed by Z20) in the eastern equatorial Pacific (see Figs. 3c, 4d). In response to the closing of the Panama Seaway, the annual-mean mixed layer depth in the eastern equatorial Pacific changes only little either, with changes on the order of a few percent of the annual-mean depth. We conclude that in the eastern equatorial Pacific, the change in mixed layer depth is much less important than that of the meridional winds. The influences of surface solar radiation (Q_S) and latent heat flux Q_E are negligible (not shown).

In summary, the enhanced equatorial asymmetry forced by the closing of the Panama Seaway is the dominant factor for amplifying the annual cycle during the course of the Pliocene. This can happen in two ways: Directly, the increased continentality to the north of the equator enhances northward meridional wind; indirectly, the strengthened AMOC

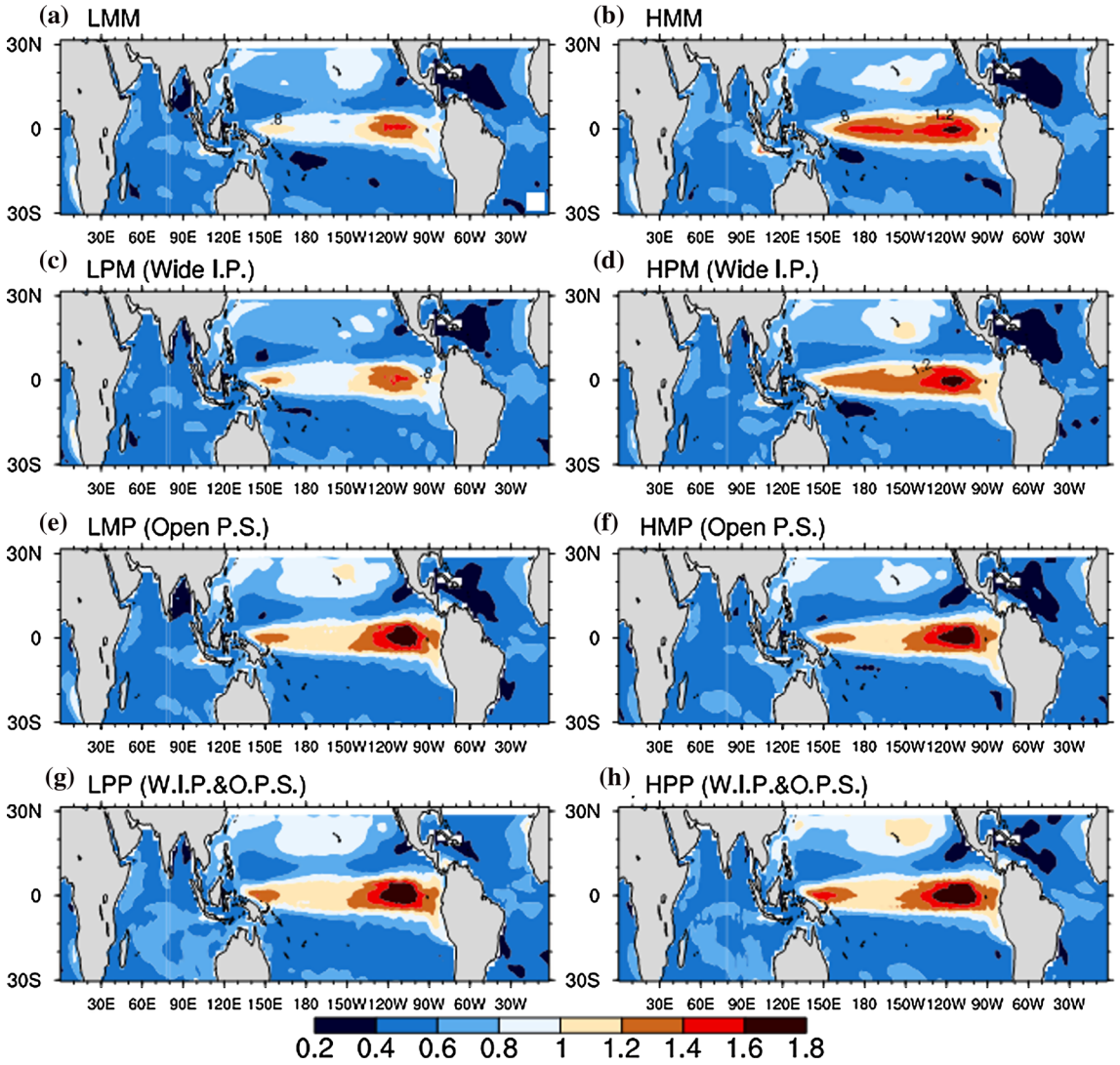

Fig. 6 SST variability (monthly standard deviation, °C) in the tropics in **a** the pre-industrial control run LMM (low-CO_2). **c**, **e**, **g** Low-CO_2 experiments with different ocean geometries. **b**, **d**, **f** The corresponding high-CO_2 experiments (*contour interval* 0.2 °C)

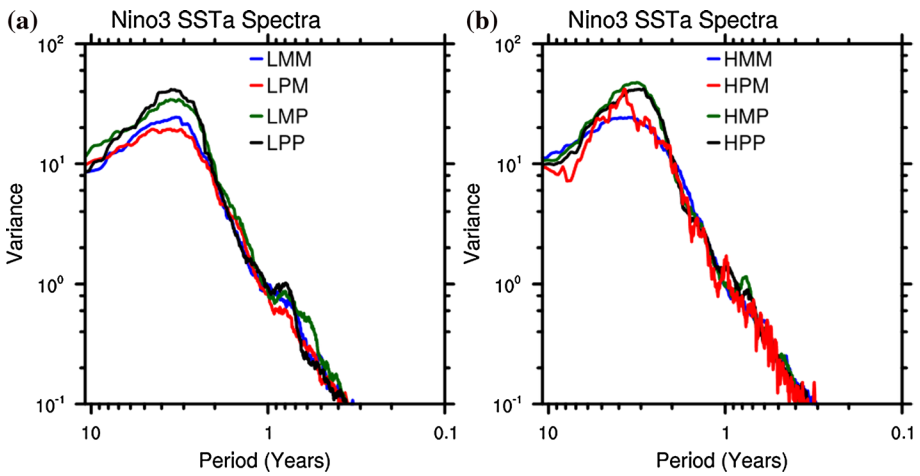

Fig. 7 Power spectra (°C^2) of SST anomalies averaged over the Niño-3 region (90°W–150°W, 5°S–5°N) in the experiments with **a** low and **b** high CO_2

warms the Northern Hemisphere through bipolar seesaw, which then affects the eastern equatorial Pacific in the same sense (Zhang and Delworth 2005; Wu et al. 2005). Our experimental setup, however, does not allow separation of these two effects. Consistent with Timmermann et al. (2004) and Huang (2015), lower CO_2-concentration weakens the annual cycle due to hemispheric cooling asymmetry.

5 ENSO stability

5.1 Linear feedbacks

In this section, we assess the stability of ENSO in the different experiments by quantifying the strength of the (linearized) positive and negative feedbacks. The first two terms in Eq. (4) are negative feedbacks which describe the dynamical and thermal damping effects on eastern equatorial Pacific SST anomalies. Dynamical damping feedback consists of three terms that are associated with mean zonal $\left(-\frac{\langle \bar{u} \rangle_E}{L_x}\right)$ and meridional currents $\left(-\frac{\langle -2y\bar{v} \rangle_E}{L_y^2}\right)$ as well as mean upwelling at the base of the mixed layer $\left(-\frac{\langle \bar{w} \rangle_E}{H_m}\right)$. Dynamical damping, ranging from -3.38 to -3.84 year^{-1}, is the dominant negative feedback in the KCM (Fig. 8a). Please note the different scales in Fig. 8. The dynamical damping, especially its upwelling component, reduces slightly in response to the narrowing of the Indonesian Passages (the difference between experiments LMM and LPM, for example, amounts to -0.07 year^{-1}). In response to the closing of the Panama Seaway, the change in dynamical damping is considerably larger (the difference between LMM and LMP, for example, amounts to about -0.25 year^{-1}). This change results from several competing factors: the spatially averaged mixed layer in the eastern box, which enters the upwelling-damping term in the denominator $\left(\propto -\frac{\langle \bar{w} \rangle_E}{H_m}\right)$, moves slightly downward due to the enhanced southerly wind stress (Fig. 4c) and reduces the damping; the meridional current-damping term increases due to the enhanced meridional SST gradient. Its magnitude, however, is small compared to that of the upwelling-damping term. The zonal currents forced by surface zonal wind stress slightly weaken, but the magnitude is also rather small. The total dynamical damping thus declines, when moving from the early Pliocene geometry towards the modern. ENSO amplitude depicts a large negative correlation with the dynamical damping, which is shown in Fig. 8a that summarizes the results from all experiments. The regression indicates that stronger ENSO would go along with stronger dynamical damping.

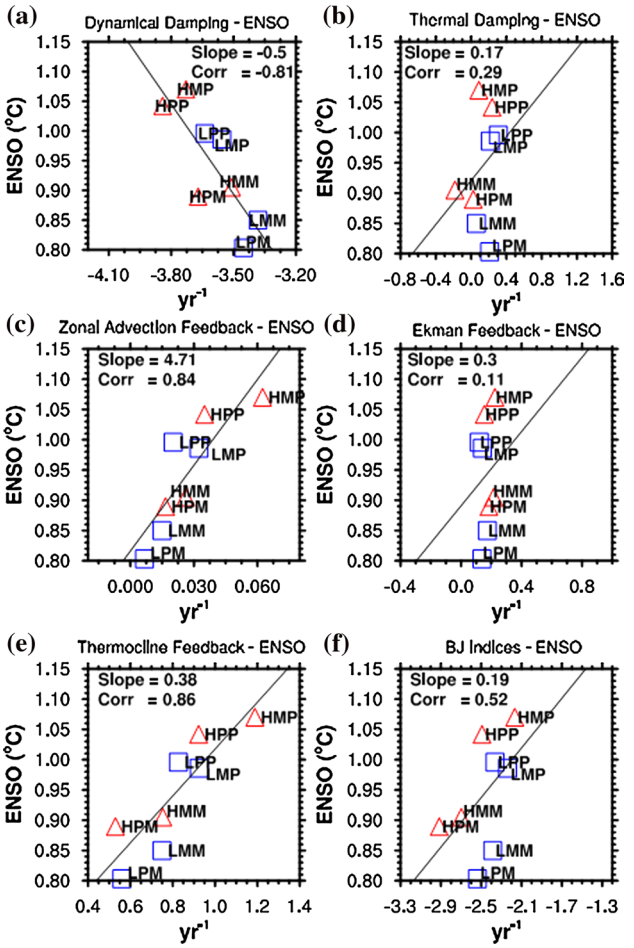

Fig. 8 Scatter plots of ENSO amplitude (°C) versus **a** dynamical damping, **b** thermal damping, **c** zonal advection feedback, **d** thermocline feedback, **e** Ekman feedback and **f** BJ index. Each component of the BJ index is converted to year^{-1}. The *black lines* depict the least square regression. ENSO amplitude is defined by the standard deviation of Niño-3 SST anomalies. *Red triangles* and *blue squares* indicate high-CO_2 and low-CO_2 experiments, respectively

The thermal damping term α is associated with the relationship between interannual anomalies of surface heat flux (shortwave, longwave, latent and sensible heat flux) and of SST in the eastern equatorial Pacific [$\langle Q \rangle_E = \alpha \langle T \rangle_E$]. It is computed as a linear least-squares regression of the net anomalous surface heat flux against SST anomalies. To compare α to other terms of the BJ Index, they are converted to a time scale by dividing by the mixed layer depth, the density and specific heat capacity of water. Compared to the dynamical damping, the thermal damping coefficients are rather small (Fig. 8b). Thus, the thermal damping is a much less important negative feedback in the KCM. Further, there is no consistent relationship of α with ENSO amplitude in the ensemble of experiments, as expressed by the rather low correlation of 0.29 (Fig. 8b).

All three positive feedbacks depend on several ocean–atmosphere coupling parameters [defined in Eqs. (5)–(8) of Jin et al. (2006)] that characterize the ocean response to surface wind stress anomalies and the atmospheric response to SST anomalies. The parameter μ_a describes the linear response of zonally averaged wind stress anomalies to forcing by eastern equatorial Pacific SST anomalies ($[\tau_x] = \mu_a \langle T \rangle_E$). Similarly, β_u and β_w characterize the linear effects of direct wind stress forcing on anomalous zonal currents and upwelling in the eastern equatorial Pacific $\left(\langle u \rangle_E = \beta_u [\tau_x] + \beta_{uh} \langle h \rangle_W, \langle H(\bar{w}) w \rangle_E = -\beta_w [\tau_x]\right)$. The coefficient β_h is estimated from the linear regression between Z20 east–west slope anomalies (defined as $\langle h \rangle_E - \langle h \rangle_W$) and the zonally averaged wind stress anomalies $\left(\langle h \rangle_E - \langle h \rangle_W = \beta_h [\tau_x]\right)$.

Consistent with the results of Kim and Jin (2011) analyzing climate models (10 out of 12 models) and Lübbecke and McPhaden (2013) analyzing observations, the dominant positive feedback in the KCM is the thermocline feedback and it depicts a rather high correlation amounting to 0.86 with ENSO amplitude (Fig. 8d). The thermocline feedback describes how eastern equatorial Pacific thermocline perturbations and thus subsurface temperature anomalies impact SST. Both the zonal advection feedback (Fig. 8c) and the Ekman feedback (Fig. 8e) are considerably smaller. The thermocline feedback weakens in response to the closing of the Panama Seaway and intensifies in response to the narrowing of the Indonesian Passages, which results from the corresponding changes in coefficients β_h and a_h. The weakening of β_h reflects the shoaling of Z20 in the eastern Pacific owing to the closing of the Panama Seaway (Fig. 3c, d). The thermocline depth, as expressed by Z20, is related to the subsurface ocean temperature. Since subsurface ocean water is actually transported into the mixed layer only when upwelling occurs, the relation is given by ($\langle H(\bar{w}) T_{sub} \rangle_E = a_h \langle h \rangle_E$) in the thermocline feedback, which follows the simple formulation of the subsurface temperature parameterization used in the Zebiak and Cane (1987) model. The parameter α_h weakens in response to the closing of the Panama Seaway, which means for the closed-Panama runs (i.e. experiments LMM and HMM) that Z20 in the eastern equatorial Pacific becomes shallower in comparison to the open-Panama runs (i.e. experiments HMP, HPP, LMP and LPP) (Fig. 4d).

The Ekman feedback is suppressed by the thermocline feedback (An and Choi 2013), since the latter modifies vertical stratification. A larger thermocline depth yields weaker stratification $\left(\left\langle -\frac{\partial \bar{T}}{\partial z} \right\rangle_E\right)$, and thus the growth rate by this effect is reduced. On the contrary, Manucharyan and Fedorov (2014) show that the Ekman feedback can even overcome the thermocline feedback in experiments with a deep thermocline depth in the eastern equatorial Pacific. The Ekman feedback becomes slightly stronger in response to the closing of the Panama Seaway (Fig. 8e).

Summing up all negative and positive feedbacks, the BJ Index is negative in all eight simulations conducted with the KCM (Fig. 8f), indicating a damped ENSO mode, with the open-Panama Seaway experiments (HMP, HPP, LMP and LPP) less damped. Notably, despite large variations in the magnitudes of the individual negative and positive feedbacks, the BJ Index is relatively constant, staying in the range from −2.3 (experiment HMP) to −1.65 (experiment LPP) year^{-1} (Fig. 8f). Comparing experiments LPM and LMM or HPM and HMM shows that the narrowing Indonesian Passages hardly modifies ENSO stability. The closing of the Panama Seaway has a much stronger effect on ENSO and reduces its amplitude. Blue squares and red triangles in Fig. 8 indicate the low-CO_2 and high-CO_2 runs, respectively. Low-CO_2-concentration yields weaker dynamical damping, zonal advection feedback and thermocline feedback, and stronger Ekman feedback. The major results, however, are basically independent of the CO_2 concentration.

We note that the computed magnitudes should be interpreted with caution in light of the accumulated errors of the various linear regressions constituting the BJ Index. Further, BJ analysis does neither account for stochastic processes nor the nonlinearities important for strong El Niño events (Graham et al. 2014). Additionally, the results depend on the size and location of the averaging box, and the selection of the depth to compute subsurface temperature anomalies. For example, we choose here the same region as in Kim and Jin (2011) to ease comparison with the BJ analysis of other climate models. Alternatively, we could have selected a smaller region such as the Niño-3 region, the region of maximum interannual SST variance. Although the calculated values may vary with the choice of the averaging box, the main findings presented above do not change, which has been confirmed by a number of sensitivity tests (not shown).

5.2 Relationship of ENSO amplitude to the annual cycle

As suggested, for example, by Liu (2002), the annual cycle tends to suppress the development of ENSO through the nonlinear mechanism of frequency entrainment. Such interaction is strongly supported by our set of model experiments, which is a major result of this study. As shown in Fig. 9, the suppression effect of the annual cycle on ENSO is clearly seen in our simulations. The correlation between the strength of the annual cycle and ENSO amplitude calculated from the eight model experiments amounts to −0.83. For example, closing the Panama Seaway induces a significantly enhanced annual cycle, largely by strengthening the meridional winds, and reduced ENSO amplitude by about 20 %. It should be noted, however, that the origin

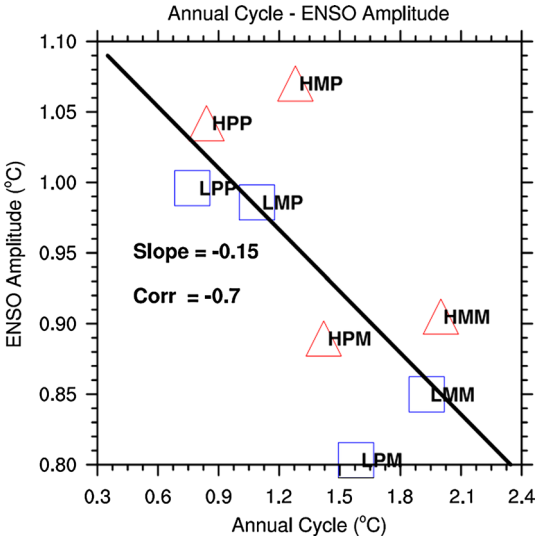

Fig. 9 Scatter plot of ENSO amplitude (°C) versus annual-cycle strength (°C). The meaning of the symbols is as in Fig. 8. The *black line* depicts the least square regression. The amplitude of the annual cycle is defined as the difference between the maximum and minimum SST in Niño-3 region (see Fig. 5)

of changes in the annual cycle and BJ index, especially the dominant thermocline feedback in the latter, are closely related to geometry changes. This hinders a clear separation of the relative importance of positive feedback and damping impact of annual cycle on ENSO variability.

6 Summary and discussion

This study investigates the impact of changes in the Panama Seaway and Indonesian Passages during the Pliocene on tropical Pacific climate and its variability. In particular, we have explored tropical Pacific mean-state and annual cycle changes, and changes in the El Niño/Southern Oscillation (ENSO) in a set of eight sensitivity simulations with the Kiel Climate Model (KCM), which differ in the geometry of the aforementioned passages and atmospheric CO_2-concentration. We studied the effect of the closing of the Panama Seaway and the narrowing of the Indonesian Passages, individually and together, using two different CO_2-concentrations.

The closing of the Panama Seaway in the KCM strongly modifies the tropical Pacific climatology. We observe shoaling of the thermocline across the tropical Pacific and strengthening of the southerly wind stress in the east, where the latter is forced by an enhanced meridional sea surface temperature (SST) gradient. A slightly decreased zonal equatorial SST gradient and zonal wind stress, indicating ocean–atmosphere coupling, is also simulated in the eastern equatorial Pacific. The strongly enhanced southerly wind stress simulated in response to the closing of the Panama Seaway is the most important factor strengthening the annual cycle. The changes in the Indonesian Passages have less impact.

We find that the simulated ENSO is relatively robust across the set of experiments. ENSO amplitude decreases in response to closing the Panama Seaway and increases in response to narrowing the Indonesian Passages [consistent with Jochum et al. (2009)]. The dominant ENSO period does not significantly change in the experiments. Higher atmospheric CO_2 enhances ENSO amplitude, consistent with Park et al. (2009) and Latif et al. (2015). As ENSO can be understood within the recharge oscillator framework, the Bjerknes stability analysis developed by Jin et al. (2006) is applied to assess changes in ocean–atmosphere feedbacks and ENSO dynamics from a linear perspective. The Bjerknes index (BJ), which sums all positive and negative feedbacks, illustrates relatively small changes across the set of experiments albeit large differences in the individual positive and negative feedbacks, which is consistent with the small but statistically significant changes in ENSO amplitude and only modest changes in ENSO period. An increase of the BJ index is accompanied by larger ENSO amplitude and vice versa.

In all experiments, dynamical damping and thermocline feedback are the dominant negative and positive feedbacks, respectively. Moreover, weakening of positive feedbacks is largely compensated by reduced dynamical damping. As a result, ENSO behavior is relatively stable across the set of experiments. Narrowing the Indonesian Passages in the model shows opposite effects in comparison to closing the Panama Seaway, and the influence of the former is much weaker. The suppression effect of the SST annual cycle on ENSO is a robust feature of the KCM: there is a clear linear relationship between the strength of the annual cycle and ENSO amplitude in the ensemble of model simulations with varying ocean geometry and atmospheric CO_2. Interestingly, changes of positive and negative feedbacks in response to closing the Panama Seaway mirror the effects of lower CO_2-concentration on these feedbacks.

Our results may provide some clues about the climate evolution from the Pliocene to the present. There are, however, several limitations in the present study. For example, when employing high atmospheric CO_2 and an open Panama Seaway, the model fails to reproduce the full extent of Pliocene warming in the mid-latitudes and upwelling regions as suggested by proxy data. This might be due to a number of physical processes not well resolved or poorly represented in the KCM. For example, variations in orbital forcing, ice sheets and vegetation distribution are not considered in the experiments. Model bias may also degrade the response.

Acknowledgments This study was supported by the Excellence Cluster "The Future Ocean" at Kiel University and the SFB 754 "Climate-Biogeochemistry Interactions in the Tropical Ocean", which both are sponsored by the German Science Foundation (DFG). The model simulations were conducted at the Computing Center of Kiel University. Zhaoyang Song is a Ph.D. student, sponsored by the Chinese Scholarship Council (CSC).

References

An S-I, Choi J (2013) Inverse relationship between the equatorial eastern Pacific annual-cycle and ENSO amplitudes in a coupled general circulation model. Clim Dyn 40(3–4):663–675. doi:10.1007/s00382-012-1403-3

Anderson DL, McCreary JP (1985) Slowly propagating disturbances in a coupled ocean–atmosphere model. J Atmos Sci 42(6):615–630. doi:10.1175/1520-0469(1985)042<0615:SPDIAC>2.0.CO;2

Bellenger H et al (2014) ENSO representation in climate models: from CMIP3 to CMIP5. Clim Dyn 42:1999–2018. doi:10.1007/s00382-013-1783-z

Bjerknes J (1969) Atmospheric teleconnections from the equatorial Pacific. Mon Weather Rev 97(3):163–172. doi:10.1175/1520-0493(1969)097<0163:ATFTEP>2.3.CO;2

Brierley CM (2015) Interannual climate variability seen in the Pliocene Model Intercomparison Project. Clim Past Discuss 10(5):3787–3820. doi:10.5194/cpd-10-3787-2014

Brierley CM, Fedorov AV, Liu Z, Herbert TD, Lawrence KT, LaRiviere JP (2009) Greatly expanded tropical warm pool and weakened Hadley circulation in the early Pliocene. Science 323(5922):1714–1718. doi:10.1126/science.1167625

Cane MA, Molnar P (2001) Closing of the Indonesian seaway as a precursor to east African aridification around 3–4 million years ago. Nature 411(6834):157–162. doi:10.1038/35075500

Chang P, Wang B, Li T, Ji L (1994) Interactions between the seasonal cycle and the Southern Oscillation-Frequency entrainment and chaos in a coupled ocean–atmosphere model. Geophys Res Lett 21(25):2817–2820. doi:10.1029/94GL02759

Cobb KM, Charles CD, Cheng H, Edwards RL (2003) El Nino/Southern Oscillation and tropical Pacific climate during the last millennium. Nature 424(6946):271–276. doi:10.1038/nature01779

Collins M et al (2010) The impact of global warming on the tropical Pacific Ocean and El Niño. Nat Geosci 3(6):391–397. doi:10.1038/ngeo868

Davies A, Kemp AE, Weedon GP, Barron JA (2012) El Niño-Southern Oscillation variability from the late cretaceous Marca shale of California. Geology 40(1):15–18. doi:10.1130/G32329.1

DiNezio PN, Kirtman BP, Clement AC, Lee SK, Vecchi GA, Wittenberg A (2012) Mean climate controls on the simulated response of ENSO to increasing greenhouse gases. J Clim 25(21):7399–7420. doi:10.1175/JCLI-D-11-00494.1

Dowsett HJ, Robinson MM, Haywood AM, Hill DJ, Dolan AM, Stoll DK, Riesselman CR (2012) Assessing confidence in Pliocene sea surface temperatures to evaluate predictive models. Nat Clim Change 2(5):365–371. doi:10.1038/nclimate1455

Fedorov AV, Dekens PS, McCarthy M, Ravelo AC, Barreiro M, Pacanowski RC, Philander SG (2006) The Pliocene paradox (mechanisms for a permanent El Niño). Science 312(5779):1485–1489. doi:10.1126/science.1122666

Fedorov AV, Brierley CM, Emanuel K (2010) Tropical cyclones and permanent El Nino in the early Pliocene epoch. Nature 463(7284):1066–1070. doi:10.1038/nature08831

Fedorov AV, Brierley CM, Lawrence KT, Liu Z, Dekens PS, Ravelo AC (2013) Patterns and mechanisms of early Pliocene warmth. Nature 496(7443):43–49. doi:10.1038/nature12003

Folland CK, Palmer TN, Parker DE (1986) Sahel rainfall and worldwide sea temperatures, 1901–85. Nature 320:602–607. doi:10.1038/320602a0

Galeotti S, Von der Heydt A, Huber M, Bice D, Dijkstra H, Jilbert T, Reichart G-J (2010) Evidence for active El Niño Southern Oscillation variability in the Late Miocene greenhouse climate. Geology 38(5):419–422. doi:10.1130/G30629.1

Graham FS, Brown JN, Langlais C, Marsland SJ, Wittenberg AT, Holbrook NJ (2014) Effectiveness of the Bjerknes stability index in representing ocean dynamics. Clim Dyn 43(9–10):2399–2414. doi:10.1007/s00382-014-2062-3

Haywood AM, Valdes PJ, Peck VL (2007) A permanent El Niño-like state during the Pliocene? Paleoceanography. doi:10.1029/2006pa001323

Haywood AM, Dowsett HJ, Robinson MM, Stoll DK, Dolan AM, Lunt DJ, Chandler MA (2011) Pliocene Model Intercomparison Project (PlioMIP): experimental design and boundary conditions (Experiment 2). Geosci Model Dev 4(3):571–577. doi:10.5194/gmd-4-571-2011

Huang P (2015) Seasonal changes in tropical SST and the surface energy budget under global warming projected by CMIP5 models. J Clim 28(16):6503–6515. doi:10.1175/JCLI-D-15-0055.1

Huber M, Caballero R (2003) Eocene El Nino: evidence for robust tropical dynamics in the "hothouse". Science 299(5608):877–881. doi:10.1126/science.1078766

Jin F-F, Neelin JD, Ghil M (1996) El Niño/Southern Oscillation and the annual cycle: subharmonic frequency locking and aperiodicity. Phys D 98:442–465

Jin F-F, Kim ST, Bejarano L (2006) A coupled-stability index for ENSO. Geophys Res Lett. doi:10.1029/2006gl027221

Jochum M, Fox-Kemper B, Molnar P, Shields C (2009) Differences in the Indonesian seaway in a coupled climate model and their relevance to Pliocene climate and El Ninõ. Paleoceanography. doi:10.1029/2008PA001678

Karas C, Nürnberg D, Gupta AK, Tiedemann R, Mohan K, Bickert T (2009) Mid-Pliocene climate change amplified by a switch in Indonesian subsurface throughflow. Nat Geosci 2(6):434–438. doi:10.1038/ngeo520

Kim ST, Jin F-F (2010a) An ENSO stability analysis. Part I: results from a hybrid coupled model. Clim Dyn 36(7–8):1593–1607. doi:10.1007/s00382-010-0796-0

Kim ST, Jin F-F (2010b) An ENSO stability analysis. Part II: results from the twentieth and twenty-first century simulations of the CMIP3 models. Clim Dyn 36(7–8):1609–1627. doi:10.1007/s00382-010-0872-5

Kim ST, Jin F-F (2011) An ENSO stability analysis. Part II: results from the twentieth and twenty-first century simulations of the CMIP3 models. Clim Dyn 36(7–8):1609–1627. doi:10.1007/s00382-010-0872-5

Krebs U, Park W, Schneider B (2011) Pliocene aridification of Australia caused by tectonically induced weakening of the Indonesian Throughflow. Palaeogeogr Palaeoclimatol Palaeoecol 309(1):111–117. doi:10.1016/j.palaeo.2011.06.002

Latif M, Keenlyside NS (2009) El Nino/Southern Oscillation response to global warming. Proc Natl Acad Sci USA 106(49):20578–20583. doi:10.1073/pnas.0710860105

Latif M, Roeckner E, Botzet M, Esch M, Haak H, Hagemann S, Jungclaus J, Legutke S, Marsland S, Mikolajewicz U, Mitchell J (2004) Reconstructing, monitoring, and predicting multidecadal-scale changes in the North Atlantic thermohaline circulation with sea surface temperature. J Clim 17:1605–1614. doi:10.1175/1520-0442(2004)017<1605:RMAPMC>2.0.CO;2

Latif M, Semenov VA, Park W (2015) Super El Niños in response to global warming in a climate model. Clim Change. doi:10.1007/s10584-015-1439-6

Li T, Philander SGH (1996) On the annual cycle of the eastern equatorial Pacific. J Clim 9(12):2986–2998. doi:10.1175/1520-0442(1996)009<2986:OTACOT>2.0.CO;2

Liu Z (1996) Modeling the equatorial annual cycle with a linear coupled model. J Clim 9:2376–2385. doi:10.1175/1520-0442(1996)009<2376:MEACWA>2.0.CO;2

Liu Z (2002) A simple model study of ENSO suppression by external periodic forcing. J Clim 15(9):1088–1098. doi:10.1175/1520-0442(2002)015<1088:ASMSOE>2.0.CO;2

Liu Z, Xie SP (1994) Equatorward propagation of coupled air–sea disturbances with application to the annual cycle of the eastern tropical Pacific. J Atmos Sci 51:3807–3822. doi:10.1175/1520-0469(1994)051<3807:EPOCAD>2.0.CO;2

Lübbecke JF, McPhaden MJ (2013) A comparative stability analysis of Atlantic and Pacific Niño modes. J Clim 26(16):5965–5980. doi:10.1175/jcli-d-12-00758.1

Lübbecke JF, McPhaden MJ (2014) Assessing the twenty-first-century shift in ENSO variability in terms of the Bjerknes stability index. J Clim 27:2577–2587. doi:10.1175/JCLI-D-13-00438.1

Madec G (2008) NEMO ocean engine. Note du Pole de modélisation 27, Institut Pierre-Simon Laplace, p 193

Maier-Reimer E, Mikolajewicz U, Crowley T (1990) Ocean general circulation model sensitivity experiment with an open Central American Isthmus. Paleoceanography 5(3):349–366. doi:10.1029/PA005i003p00349

Manucharyan GE, Fedorov AV (2014) Robust ENSO across a wide range of climates. J Clim 27(15):5836–5850. doi:10.1175/jcli-d-13-00759.1

McGregor S, Timmermann A, England MH, Elison Timm O, Wittenberg AT (2013) Inferred changes in El Niño-Southern Oscillation variance over the past six centuries. Clim Past Discuss 9(5):2269–2284. doi:10.5194/cp-9-2269-2013

Mechoso CR et al (1995) The seasonal cycle over the tropical Pacific in coupled ocean–atmosphere general circulation models. Mon Weather Rev 123:2825–2838. doi:10.1175/1520-0493(1995)123<2825:TSCOTT>2.0.CO;2

Pagani M, Liu Z, LaRiviere J, Ravelo AC (2009) High earth-system climate sensitivity determined from Pliocene carbon dioxide concentrations. Nat Geosci 3(1):27–30. doi:10.1038/ngeo724

Park W, Keenlyside N, Latif M, Ströh A, Redler R, Roeckner E, Madec G (2009) Tropical Pacific climate and its response to global warming in the Kiel climate model. J Clim 22(1):71–92. doi:10.1175/2008jcli2261.1

Roeckner E, Bäuml G, Bonaventura L, Brokopf R, Esch M, Giorgetta M, Manzini E (2003) The atmospheric general circulation model ECHAM5. Part I: model description. Max Planck Institute for Meteorology, Hamburg, Germany, Report No. 349, p 127

Scroxton N, Bonham SG, Rickaby RE, Lawrence SHF, Hermoso M, Haywood AM (2011) Persistent El Niño-Southern Oscillation variation during the Pliocene Epoch. Paleoceanography. doi:10.1029/2010PA002097

Timmermann A, Jin FF, Collins M (2004) Intensification of the annual cycle in the tropical Pacific due to greenhouse warming. Geophys Res Lett. doi:10.1029/2004GL019442

Timmermann A, Okumura Y, An SI, Clement A, Dong B, Guilyardi E, Yin J (2007) The influence of a weakening of the Atlantic meridional overturning circulation on ENSO. J Clim 20(19):4899–4919. doi:10.1175/jcli4283.1

Valcke S (ed) (2006) OASIS3 user guide. PRISM Tech. Rep. 3. http://www.prism.enes.org/Publications/Reports/oasis3_UserGuide_T3.pdf

Vecchi GA, Soden BJ (2007) Global warming and the weakening of the tropical circulation. J Clim 20(17):4316–4340. doi:10.1175/JCLI4258.1

Wara MW, Ravelo AC, Delaney ML (2005) Permanent El Nino-like conditions during the Pliocene warm period. Science 309(5735):758–761. doi:10.1126/science.1112596

Watanabe T, Suzuki A, Minobe S, Kawashima T, Kameo K, Minoshima K, Kase T (2011) Permanent El Nino during the Pliocene warm period not supported by coral evidence. Nature 471(7337):209–211. doi:10.1038/nature09777

Wu L, He F, Liu Z (2005) Coupled ocean–atmosphere response to tropical North Atlantic SST variability: tropical Atlantic Dipole and ENSO. Geophys Res Lett 32:L21712. doi:10.1029/2005GL024222

Xie S-P (1994) On the genesis of the equatorial annual cycle. J Clim 7:2008–2013. doi:10.1175/1520-0442(1994)007<2008:OTGOTE>2.0.CO;2

Xie S-P (1996) Westward propagation of latitudinal asymmetry in a coupled ocean–atmosphere model. J Atmos Sci 53:3236–3250. doi:10.1175/1520-0469(1996)053<3236:WPOLAI>2.0.CO;2

Xie SP, Kubokawa A, Hanawa K (1989) Oscillations with two feedback processes in a coupled ocean–atmosphere model. J Clim 2(9):946–964. doi:10.1175/1520-0442(1989)002<0946:OWTFPI>2.0.CO;2

Zebiak SE, Cane MA (1987) A model EI Nino-Southern Oscillation. Mon Weather Rev 115:2262–2278. doi:10.1175/1520-0493(1987)115<2262:AMENO>2.0.CO;2

Zhang R, Delworth T (2005) Simulated tropical response to a substantial weakening of the Atlantic thermohaline circulation. J Clim 18:1853–1860. doi:10.1175/JCLI3460.1

Zhang X, Prange M, Steph S, Butzin M, Krebs U, Lunt DJ, Schulz M (2012) Changes in equatorial Pacific thermocline depth in response to Panama seaway closure: insights from a multi-model study. Earth Planet Sci Lett 317:76–84. doi:10.1016/j.epsl.2011.11.028